Stabilization of s-wave superconductivity through arsenic p-orbital hybridization in electron-doped BaFe_{2}As_{2}

David W. Tam, Tom Berlijn, and Thomas A. Maier

Phys. Rev. B **98**, 024507 — Published 12 July 2018

DOI: 10.1103/PhysRevB.98.024507

Stabilization of s-wave superconductivity through arsenic p-orbital hybridization in electron-doped $BaFe_2As_2$

David W. Tam,[1] Tom Berlijn,[2] and Thomas A. Maier[2,*]

[1]*Department of Physics and Astronomy, Rice University, Houston, Texas 77005, USA*
[2]*Center for Nanophase Materials Sciences and Computational Science and Engineering Division, Oak Ridge National Laboratory, Oak Ridge, Tennessee 37831-6494, USA*

(Dated: June 20, 2018)

Using random-phase approximation spin-fluctuation theory, we study the influence of the hybridization between iron d-orbitals and pnictide p-orbitals on the superconducting pairing state in iron-based superconductors. The calculations are performed for a 16-orbital Hubbard-Hund tight-binding model of $BaFe_2As_2$ that includes the As-p orbital degrees of freedom in addition to the Fe-d orbitals and compared to calculations for a 10-orbital Fe-d only model. In both models we find a leading $s^{\pm}$ pairing state and a subleading $d_{x^2-y^2}$-wave state in the parent compound. Upon doping, we find that the $s^{\pm}$ state remains the leading state in the 16-orbital model up to a doping level of 0.475 electrons per unit cell, at which the hole Fermi surface pockets at the zone center start to disappear. This is in contrast to the 10-orbital model, where the d-wave state becomes the leading state at a doping of less than 0.2 electrons. This improved stability of $s^{\pm}$ pairing is found to arise from a decrease of d_{xy} orbital weight on the electron pockets due to hybridization with the As-p orbitals and the resulting reduction of near (π,π) spin-fluctuation scattering which favors the competing d-wave state. These results show that the orbital dependent hybridization of Fermi surface Bloch states with the usually neglected p-orbital states is an important ingredient in an improved itinerant pairing theory.

PACS numbers: 74.70.Xa, 74.20.Rp, 74.20.Fg, 74.25.Jb

The detailed nature of the pairing mechanism that gives rise to superconductivity in the iron-based superconductors continues to be a matter of debate. Based on the proximity of the superconducting state to the magnetic stripe order observed in most parent and weakly doped materials, antiferromagnetic spin fluctuations have been widely discussed to play a major role. Early on it was predicted that these fluctuations, occuring at a wavevector $Q = (\pi, 0)$ that separates the Fermi surface hole pockets at the zone center and the electron pocket at $(\pi, 0)$, will mediate an $s^{\pm}$ superconducting state, in which the gap changes sign between the hole and electron pockets [1].

Given the metallic character of the iron-based parent compounds, a weak-coupling fluctuation exchange picture is a natural platform for understanding superconductivity in these systems. Random phase approximation (RPA) based spin-fluctuation calculations for realistic tight-binding models of these systems indeed find an $s^{\pm}$ superconducting state [2]. However, these calculations also suggest a strongly competitive $d_{x^2-y^2}$ pairing channel [3, 4], which can even become dominant with either electron or hole doping. In fact, for certain cases, this transition from an s-wave to a d-wave ground state happens already at very small levels of electron doping. Fig. 1, for example, displays the results of an RPA calculation for a three dimensional (3D) 10-orbital model (2 Fe per unit cell) of $BaFe_2As_2$, where this change already occurs at a doping level of 0.1 electrons per Fe. Experimentally, the existence of an s-wave superconducting gap in doped $BaFe_2As_2$ is broadly supported by experiments including ARPES, muon spin relaxation, optical reflectivity, heat capacity, neutron scattering, and other techniques [5–8]. However, there is no evidence for a change to d-wave gap symmetry at small doping levels.

This problem of spin-fluctuation RPA theory is intimately linked to the momentum structure of the spin-fluctuation interaction. For systems with both hole- and electron pockets of approximately equal size such as in the parent compounds, the RPA spin susceptibility is dominated by a strong peak at $Q = (\pi, 0)$, which arises from the nesting between the hole pockets and the electron pockets and which favors the $s^{\pm}$ state. But additional scattering between opposite sides of the electron pockets gives rise to a ridge-like structure around (π, π), which becomes dominant already at small levels of electron doping and which favors the d-wave state [9].

The low-temperature phase of optimally superconducting $BaFe_2As_2$ crystallizes with tetragonal I4/mmm symmetry containing an inversion center. This gives rise to two distinct iron sublattices and, as a result, a model containing ten iron-d orbitals (five each for the two inequivalent iron sites in the unit cell) is the minimal model required to generate the appropriate orbital eigenstates at the Fermi energy.

In this work, we show that by including the six inequivalent arsenic p orbitals in addition to the ten iron d orbitals, the competing d-wave pairing state is suppressed and the $s^{\pm}$ state remains the leading pairing state up to an electron doping level where the hole pocket disappears and low energy spin-fluctuations near $(\pi, 0)$ are suppressed. These results suggest that the hybridization

of the d-orbitals with the arsenic p states, despite their relatively small spectral weight at the Fermi energy, is an important factor in a complete picture of superconductivity in these materials.

Iron in $BaFe_2As_2$ is nominally in the 2+ oxidation state, leaving a $3d^6$ shell (12.0 carrier electrons per two-iron unit cell); optimal SC occurs at $BaFe_{1.9}Ni_{0.1}As_2$, corresponding to a donation of two electrons per $3d^8$ Ni (12.2 carriers), while SC is extinguished near $BaFe_{1.75}Ni_{0.25}As_2$ (12.5 carriers). For the 16-orbital models, As takes the 3- state, yielding $4p^6$ and contributing an extra 12 carriers per unit cell; $BaFe_{1.9}Ni_{0.1}As_2$ then corresponds to 24.2 carriers. We use the WIEN2K software package [10] to generate multi-orbital tight-binding models for the parent (undoped) compounds using the experimentally-determined lattice positions of the As ions, which we project into a tight-binding Wannier basis with WIEN2WANNIER [11] and WANNIER90 [12]. From these models, our methods proceed as described before [3, 4, 13–17], first calculating the bare magnetic susceptibility tensor

$$\chi^0_{\ell_1\ell_2\ell_3\ell_4}(\mathbf{q},\omega) = -\frac{1}{N}\sum_{\mathbf{k},\mu\nu} \frac{a_\mu^{\ell_4}(\mathbf{k})a_\mu^{\ell_2,*}(\mathbf{k})a_\nu^{\ell_1}(\mathbf{k}+\mathbf{q})a_\nu^{\ell_3,*}(\mathbf{k}+\mathbf{q})}{\omega + E_\mu(\mathbf{k}) - E_\nu(\mathbf{k}+\mathbf{q}) + i\delta} \left[f(E_\mu(\mathbf{k}),T) - f(E_\nu(\mathbf{k}+\mathbf{q}),T)\right] \quad , \tag{1}$$

with the band indices μ and ν, and orbital indices ℓ_i. The matrix elements $a_\mu^\ell(\mathbf{k}) = \langle \ell|\mu\mathbf{k}\rangle$ represent the orbital projection of the Bloch states, $f(E_\mu(\mathbf{k}),T)$ is the Fermi function for band energy $E_\mu(\mathbf{k})$ at temperature T which we set to $100K$. For the sum over $\mathbf{k}$ we use a mesh of $40\times40\times4$ points over the 3D Brillouin zone. We then compute the RPA spin and charge susceptibility tensors

$$\chi^{s/c,\mathrm{RPA}}_{\ell_1\ell_2\ell_3\ell_4}(\mathbf{q},\omega) = \left\{\chi^0(\mathbf{q},\omega)[1-\mathcal{U}^{s/c}\chi^0(\mathbf{q},\omega)]^{-1}\right\}_{\ell_1\ell_2\ell_3\ell_4} \tag{2}$$

using the interaction matrices in orbital space for the spin ($\mathcal{U}^s$) and charge ($\mathcal{U}^c$) channels, which contain linear combinations of intra- and inter-orbital Coulomb repulsions U and U', respectively, as well as Hund's rule and pair-hopping terms J and J', respectively [4]. We have used spin rotational invariant combinations that satisfy $U' = U/2$ and $J = J' = U/4$ [18]. We find that adjusting the ratios of the Coulomb interaction parameters, such as the choice $J = U/10$, has no effect on the conclusions of this work, except to scale the RPA susceptibility and pairing eigenvalues. We choose different values for U for the 10- and 16-orbital models (keeping the parameter ratios fixed) as explained below. The physical spin susceptibility is then given by

$$\chi^{s,\mathrm{RPA}}(\mathbf{q},\omega) = \frac{1}{2}\sum_{\ell_1\ell_2}\chi^{s,\mathrm{RPA}}_{\ell_1\ell_1\ell_2\ell_2}(\mathbf{q},\omega)\,. \tag{3}$$

The superconducting properties are calculated from the pairing vertex in band representation

$$\Gamma_{ij}(\mathbf{k},\mathbf{k}') = \mathrm{Re}\sum_{\ell_1\ell_2\ell_3\ell_4} a_{\nu_i}^{\ell_1,*}(\mathbf{k})a_{\nu_i}^{\ell_4,*}(-\mathbf{k}) \times \Gamma_{\ell_1\ell_2\ell_3\ell_4}(\mathbf{k},\mathbf{k}',\omega=0)a_{\nu_j}^{\ell_2}(\mathbf{k}')a_{\nu_j}^{\ell_3}(-\mathbf{k}')\,, \tag{4}$$

where the momenta $\mathbf{k}\in\mathcal{C}_i$ and $\mathbf{k}'\in\mathcal{C}_j$ are restricted to the electron and hole Fermi surface sheets $\mathcal{C}_{i/j}$ and $\nu_{i/j}$ are the band indices of these sheets. The scattering vertex $\Gamma_{\ell_1\ell_2\ell_3\ell_4}$ describes the particle-particle scattering in orbital space and is given in RPA approximation as

$$\Gamma_{\ell_1\ell_2\ell_3\ell_4}(\mathbf{k},\mathbf{k}',\omega) = \Big[\frac{3}{2}\mathcal{U}^s\chi^s_{\mathrm{RPA}}(\mathbf{k}-\mathbf{k}',\omega)\mathcal{U}^s + \frac{1}{2}\mathcal{U}^s - \frac{1}{2}\mathcal{U}^c\chi^c_{\mathrm{RPA}}(\mathbf{k}-\mathbf{k}',\omega)\mathcal{U}^c + \frac{1}{2}\mathcal{U}^c\Big]_{\ell_1\ell_2\ell_3\ell_4}\,. \tag{5}$$

The momentum structure $g(k)$ of the pairing state can then be found by solving the eigenvalue problem [4]

$$-\sum_j \oint_{C_j} \frac{d\mathbf{k}'_\parallel}{2\pi v_F(\mathbf{k}'_\parallel)}\Gamma_{ij}(\mathbf{k},\mathbf{k}')g_\alpha(\mathbf{k}') = \lambda_\alpha g_\alpha(\mathbf{k}) \tag{6}$$

where the eigenfunction $g_\alpha(\mathbf{k})$ corresponding to the largest eigenvalue λ_α gives the leading pairing instability of the system. We calculate the pairing states for different electron dopings by applying a rigid band shift.

For the undoped case (12 electrons per unit cell), we generally find a leading s-wave solution with $s^\pm$ structure where the gap changes sign between hole and electron pockets. In both the 10- and 16-orbital models, the gap is fairly isotropic on the hole pockets and displays similar angular variation on the electron pockets but is nodeless. The second leading solution we observe in the 10-orbital model has $d_{x^2-y^2}$ structure with nodes on both the hole and electron pockets (due to hybridization of the latter). In the 16-orbital model, we also observe this $d_{x^2-y^2}$ state, but, in addition, there are other d-wave solutions (including d_{xy}) with larger eigenvalues. Since these other states rapidly disappear with electron doping we ignore them in the following discussion and focus on the doping dependence of $s^\pm$ and $d_{x^2-y^2}$-wave states.

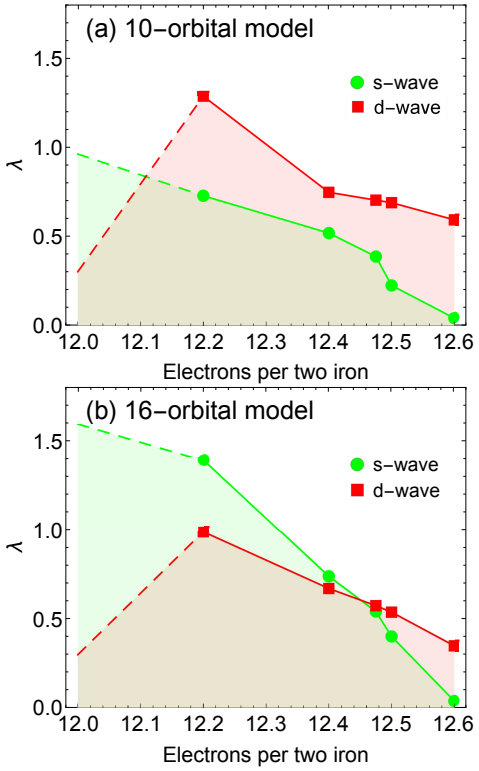

FIG. 1: Pairing eigenvalues for the 10-orbital (a) and 16-orbital model (b) for electron-doped $BaFe_2As_2$ using a rigid band shift. The parent compound has $\langle n \rangle = 12.0$ electrons per two iron, whereas $\langle n \rangle$ =12.5 corresponds to a nominal doping of $BaFe_{1.75}Ni_{0.25}As_2$ or $BaFe_{1.5}Co_{0.5}As_2$. The dashed lines show that different RPA interactions are used for the undoped compounds that give eigenvalues close to 1.

Fig. 1 shows the doping dependence of the $s^{\pm}$ and d-wave eigenvalues for the 10-orbital model, which does not include the arsenic orbitals, and the full 16-orbital model that includes the three (per arsenic) p-orbitals. In the moderate to strong doping regime (12.2/24.2 electrons per unit cell and higher), the RPA interactions are chosen to generate eigenvalues roughly in the range 0 to 1; we use $U = 1.10$ and 1.72 for the 10- and 16-orbital models, respectively. The fact that a larger interaction U needs to be chosen to give similar pairing strengths in the 16-orbital model reflects the fact that the additional screening from the p-orbitals is not included in the bare interaction parameters of the 16-orbital models. Using the same interaction parameter U for the parent compound (12.0/24.0 electrons per unit cell) would lead to an antiferromagnetic spin-density wave instability at $(\pi, 0)$. In order to suppress this instability and study the order of the leading pairing solutions in this regime, we choose a different U for the undoped case. For the 10-orbital model we set $U = 0.92$ and choose 1.40 for the 16-orbital model. This choice gives the same d-wave eigenvalues $\lambda_d = 0.3$ for both models.

With this choice of interaction parameters, we find that the $s^{\pm}$ state is the leading instability in the undoped case for both models, but the margin by which it is leading over the d-wave state is much larger in the 16-orbital model than in the 10-orbital model. Most importantly in the 16-orbital model the $s^{\pm}$ state remains the leading state up to a doping of approximately 0.475 electrons per unit cell. In contrast, in the 10-orbital model, the d-wave state becomes the leading state already at a doping of less than 0.2 electrons per unit cell.

In order to understand this significant increase in the stability of the $s^{\pm}$ state over the d-wave state in the 16-orbital model, we now examine the momentum structure of the zero frequency RPA spin susceptibility $\chi^{s,\mathrm{RPA}}(\mathbf{q}, \omega = 0)$ (Eq. (3)), which enters the paring interaction Eq. (5). Fig. 2 shows $\chi^{s,\mathrm{RPA}}(\mathbf{q}, \omega = 0)$ for $\mathbf{q}$ along high symmetry directions in the 1 Fe/unit cell Brillouin zone for different dopings in the 10-orbital (a) and 16-orbital (b) models. As noted before, the spin-fluctuation scattering at $(\pi, 0)$ favors the $s^{\pm}$ pairing state, while the d-wave state arises from scattering near (π, π). For the undoped case, one sees a peak at $(\pi, 0)$ for both the 10-orbital and the 16-orbital models, leading to the dominant $s^{\pm}$ state that is found in Fig. 1. However, this peak is much more enhanced over the scattering near (π, π) in the 16-orbital model than in the 10-orbital case. This explains the larger difference between the $s^{\pm}$ and the d-wave eigenvalues in the 16-orbital model at half-filling. As the doping increases, one sees that the $(\pi, 0)$ peak relative to the (π, π) peak diminishes slower in the 16-orbital model than in the 10-orbital model. For example at $x = 0.2$ the susceptibility maximum is no longer at $(\pi, 0)$ in the 10-orbital model, whereas in the 16-orbital model it still is. As a result, the $s^{\pm}$ state remains more stable with increasing doping and dominant over the d-wave up to a doping level of ~ 0.475 electrons.

This doping corresponds exactly with the filling where the Fermi surface hole pockets at the zone center start to disappear. Fig. 3 shows the Fermi surface of the 16-orbital model for a filling of 12.4 (a) and 12.475 (b) and one sees that the hole pockets at the zone center are disappearing for a filling of 12.475. The fact that the d-wave pairing state becomes leading at this doping is a consequence of our Fermi surface restricted treatment of the pairing problem, since the low energy spin fluctuations near $(\pi, 0)$ that favor the $s^{\pm}$ state are suppressed when the hole bands move below the Fermi energy. This is shown in the bottom panel in Fig. 3, where we plot the real part of the RPA spin susceptibility $\mathrm{Re}\,\chi^{s,\mathrm{RPA}}(\mathbf{q}, \omega = 0)$ for different dopings. Here we have integrated the susceptibility over small 2D regions of size $(0.2\pi, 0.2\pi)$ around the nominal position, and averaged over q_z, although we find little difference for any single q_z. In the 10-orbital model, upon doping, the (π, π) scattering immediately becomes much stronger than the $(\pi, 0)$ scattering. In contrast, in the 16-orbital model the $(\pi, 0)$ scattering remains dominant up to a doping of 0.25 elec-

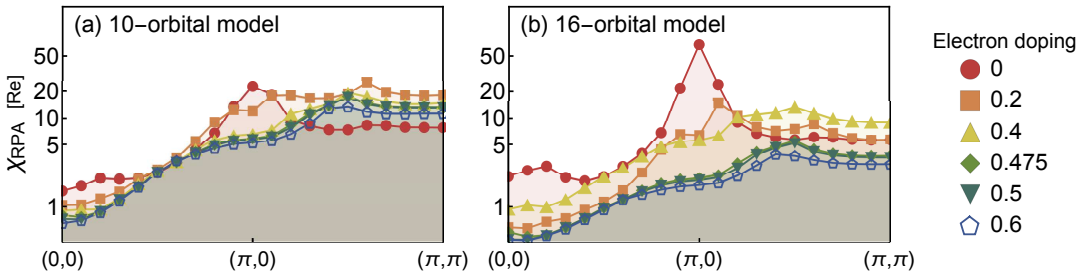

FIG. 2: (Note log scale) Cuts of the RPA susceptibility along high-symmetry directions in the 1 Fe/unit cell Brillouin zone, for the electron-doped system, and for the 10-orbital (a) and 16-orbital (b) models. The RPA interaction U is chosen just below the critical strength that leads to a divergence of $\chi_{\rm RPA}$. This divergence occurs at U=1.19 for the 10-orbital model, and 1.73 for the 16-orbital model, for 12.2 electrons per iron in both cases. For the parent compounds, interactions are chosen to give pairing eigenvalues close to 1.

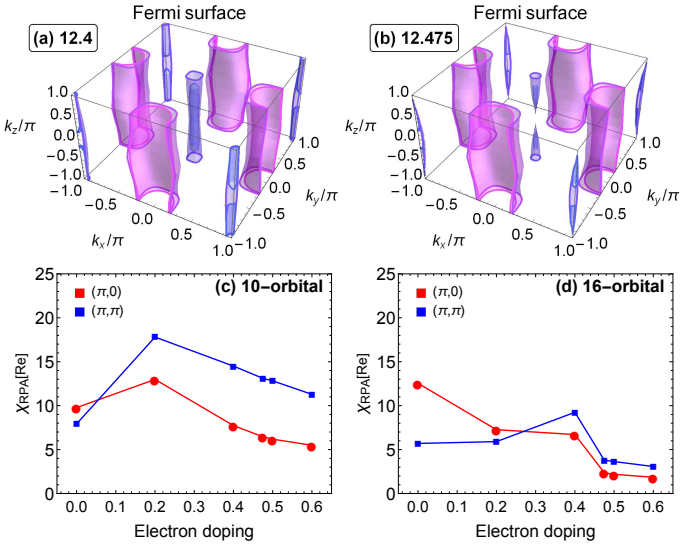

FIG. 3: Fermi surface in the 16-orbital model for a filling of 12.4 electrons (a) and 12.475 electrons (b) per uni cell. Doping dependence of the RPA spin susceptibility $\chi^{s,\rm RPA}(\mathbf{q},\omega=0)$ for $\mathbf{q}$ near $(\pi,0)$ and (π,π) in the (c) 10-orbital and (d) 16-orbital model. The Fermi surfaces in (a-b) are for the 16-orbital model but are found to be indistinguishable from those in the 10-orbital model.

trons, and for higher doping the two regions show very similar magnitude. We also find that the spin gap at $(\pi,0)$ in the imaginary part of $\chi(\mathbf{q},\omega)$ also increases significantly upon crossing the threshold of 12.475 electrons, and spectral weight is transferred to higher energies upon further doping. This is similar to what is observed in neutron scattering experiments. Data on $BaFe_{1.7}Ni_{0.3}As_2$, which corresponds to nominally 24.6 electrons per unit cell, shows that a spin gap remains open and the spectral weight has shifted upward to 60 meV [19]. In our calculations in the 16-orbital model, we find a spin gap of about 30 meV at 0.4 electrons is pushed upwards to nearly 60 meV at 0.475 electrons. This agreement suggests that the low-energy dynamics may be well represented in our model.

Moreover we note that, experimentally, the critical doping $x \approx 0.25$ at which T_c goes to zero in $BaFe_{2-x}Ni_xAs_2$ corresponds to nominally 24.5 electrons per unit cell. Thus we find witin the 16-orbital model, that the $s^{\pm}$ state is the leading pairing state over almost the full superconducting dome in Ni-doped $BaFe_2As_2$. We further note that a full theory that takes into account the dynamics of the interaction would pick up the spectral weight in the spin fluctuation spectrum at higher energies and thus likely extend the doping range over which the $s^{\pm}$ state is dominant [20, 21].

In order to better understand how the arsenic p-orbitals give rise to this behavior, we calculate the orbital contributions to the the Fermi surface Bloch states

$$w_i^\ell = \int_{\mathcal{C}_i} \frac{d\mathbf{k}}{(2\pi)^2} \left|a_\mu^\ell(\mathbf{k})\right|^2 . \qquad (7)$$

Here the integral is over the Fermi surface momenta of sheet i and μ is the band index of the sheet.

In Fig. 4 we plot the orbital weights w_i^ℓ for both the 10-orbital (dashed outline) and the 16-orbital (solid outline) model summed over the different hole pockets (a) and electron pockets (b). In the 16-orbital model, one observes that the arsenic p-orbitals hybridize with all of the iron d-orbitals, reducing the orbital content of all 5 d-orbitals on the Fermi surface states. The most significant change in terms of total orbital weight is the reduction of the d_{xy} content on the electron pockets. Also shown in Fig. 4 are the largest intra-orbital contributions $(\ell_1=\ell_2)$ to the spin susceptibility $\chi^0(\mathbf{q},\omega=0)$ in Eq. (1) for both the 10-orbital and 16-orbital models. From this one sees that that the $(\pi,0)$ peak in $\chi^0(\mathbf{q},\omega=0)$ arises mainly from scattering between the d_{yz} orbitals on the hole and electron pockets, while the d_{xy} contribution is dominant in the near (π,π) scattering. Relative to the 10-orbital model, the d_{xy} scattering is reduced more than the d_{yz} scattering, consistent with the larger reduction of the xy orbital weights on the electron pockets. Hence, it is the fact that the arsenic p-orbitals have the strongest

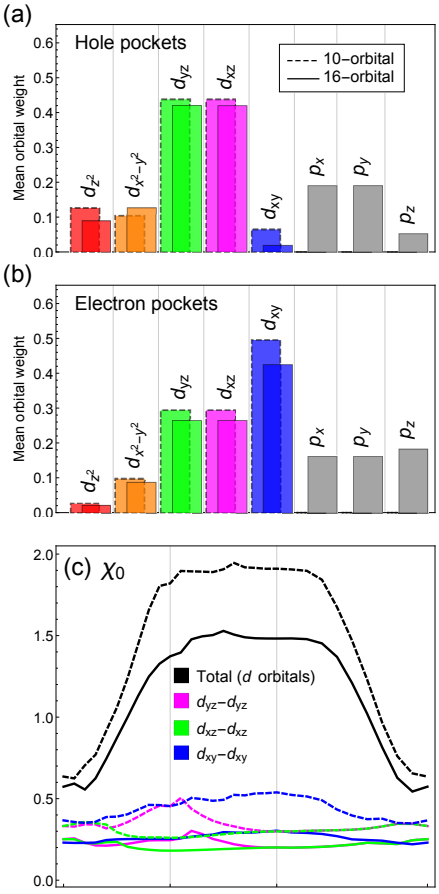

FIG. 4: (a-b) Orbital weights of the Fermi surface Bloch states for 12.4 electrons per two iron atoms (overdoped; $BaFe_{1.8}Ni_{0.2}As_2$) for the 10- (dashed borders) and 16-orbital models (solid borders). (a): Orbital weights for the two Γ-centered hole pockets. (b): Orbital weights for the two electron pockets. The reduction in d_{xy} intensity on the electron pockets leads to a reduction of the spin susceptibility near the wavevector (π,π) connecting them. (c) Bare (noninteracting) susceptibility χ_0 and intra-orbital $\chi_0^{\ell_1,\ell_1,\ell_1,\ell_1}$ for $\ell_1 = d_{xz}$,d_{yz}, and d_{xy}, for the 10-orbital (dashed) and 16-orbital model (solid).

hybridization with the d_{xy} orbitals on the electron pockets that leads to the reduction of the near (π,π) spin-fluctuation scattering and ultimately to the increased stability of the $s^{\pm}$ pairing state with electron doping.

To summarize, we have carried out RPA spin-fluctuation calculations of the spin susceptibility and the leading pairing states in a 16-orbital Hubbard-Hund tight-binding model of electron-doped $BaFe_2As_2$. In addition to the 10 Fe-d orbitals per unit cell, this model includes the 6 p-orbitals from the As atoms and their hybridization with the d-orbitals. We have compared the results of these calculations with those of a Fe-d, 10-orbital only model that does not include the As-p degrees of freedom. In both models we find a leading $s^{\pm}$ pairing state and a subleading $d_{x^2-y^2}$-wave state in the parent compound. Upon doping, the 10-orbital model has the d-wave state become the leading state already at an electron doping level of less than 0.2 electrons per unit cell. In contrast, in the 16-orbital model the $s^{\pm}$ state is much more stable and remains the leading pairing state and dominant over the d-wave state up to doping levels of 0.475 electrons. At this doping level, the hole Fermi surface pockets at the zone center are found to disappear. The increased stability of the $s^{\pm}$ over the d-wave state is found to arise from an increased ratio of the strength of spin-fluctuation scattering near $q = (\pi, 0)$ which connects hole- and electron pockets and $q = (\pi,\pi)$ which connects the electron pockets. This reduction of the near (π,π) scattering is found to be unrelated to a change in the Fermi surface shape, which is nearly identical between the 10- and 16-orbital models, but rather can be traced to a decrease in the d_{xy} orbital weight on the electron pockets due to their hybridization with the As-p degrees of freedom.

Orbital selectivity, i.e. the orbital dependent coherence of quasiparticles, has been argued to play a major role in the Cooper pairing in iron-based superconductors [22–25]. In particular, Kreisel et al. [24] have found that the incorporation of quasiparticle weight factors can modify the results of RPA spin-fluctuation calculations of the pairing state via suppression of the pair scattering processes involving the less coherent d_{xy} states. Here we have shown that the orbital dependent hybridization of Fermi surface Bloch states with the usually neglected p-orbital states provides another, complementary ingredient for an improved itinerant pairing theory.

Acknowledgements

The RPA calculations in this work have been supported by NSF under grant NSF-DMR-1308603 (D.W.T.). The analysis and interpretation of the results (T.A.M.) and the DFT and Wannier function calculations (T.B.) were supported by the U.S. Department of Energy, Office of Basic Energy Sciences, Materials Sciences and Engineering Division.

* Electronic address: maierta@ornl.gov

[1] I. I. Mazin, D. J. Singh, M. D. Johannes, M. H. Du, M. H. Phys. Rev. Lett. 101, 057003 (2008).
[2] P. J. Hirschfeld, Comptes Rendus Physique (2015).
[3] K. Kuroki, S. Onari, R. Arita, H. Usui, Y. Tanaka, H. Kontani, and H. Aoki, Phys. Rev. Lett. 101, 087004 (2008).
[4] S. Graser, T.A. Maier, P.J. Hirschfeld, and D.J. Scalapino, New J. Phys. **11**, 025016 (2009).
[5] P.J. Hirschfeld, M.M. Korshunov, and I.I. Mazin, Rep. Prog. Phys. **74**, 124508 (2011).

[6] K. Terashima, Y. Sekiba, J.H. Bowen, K. Nakayama, T. Kawahara, T. Sato, P. Richard, Y.-M. Xu, L.J. Li, G.H. Cao, Z.-A. Xu, H. Ding, and T. Takahashi, Proc Natl Acad Sci U S A **106**, 7330 (2009).

[7] D.C. Johnston, Advances in Physics **59**, 803 (2010).

[8] A.A. Aczel, E. Baggio-Saitovitch, S.L. Budko, P.C. Canfield, J.P. Carlo, G.F. Chen, P. Dai, T. Goko, W.Z. Hu, G.M. Luke, J.L. Luo, N. Ni, D.R. Sanchez-Candela, F.F. Tafti, N.L. Wang, T.J. Williams, W. Yu, and Y.J. Uemura, Phys. Rev. B **78**, 214503 (2008).

[9] R. M. Fernandes and A. J. Millis, Phys. Rev. Lett. **110**, 117004 (2013).

[10] K. Schwarz, P. Blaha, and G. K. H. Madsen, Comput. Phys. Commun. 147, 71 (2002).

[11] Jan Kuneš, Ryotaro Arita, Philipp Wissgotte, Alessandro Toschie, Hiroaki Ikedaf, Karsten Helde, Computer Physics Communications **181**, Issue 11, 1888-1895 (2010).

[12] A. A. Mostofi, J. R. Yates, Y.-S. Lee, I. Souza, D. Vanderbilt and N. Marzari, Comput. Phys. Commun. 178, 685 (2008).

[13] T. Maier and D. Scalapino, Physical Review B **78**, 020514 (2008).

[14] T. Maier, S. Graser, D. Scalapino, and P. Hirschfeld, Physical Review B **79**, 134520 (2009).

[15] T.A. Maier, S. Graser, P.J. Hirschfeld, and D.J. Scalapino, Phys. Rev. B **83**, 100515 (2011).

[16] T.A. Maier, P.J. Hirschfeld, and D.J. Scalapino, Physical Review B **86**, 094514 (2012).

[17] Y. Wang, A. Kreisel, V. Zabolotnyy, S. Borisenko, B. Büchner, T. Maier, P. Hirschfeld, and D. Scalapino, Phys. Rev. B **88**, 174516 (2013).

[18] C. Noce and A. Romano, Phys. Status Solidi B **251**, 907 (2014).

[19] M. Wang, C. Zhang, X. Lu, G. Tan, H. Luo, Y. Song, M. Wang, X. Zhang, E.A. Goremychkin, T.G. Perring, T.A. Maier, Z. Yin, K. Haule, G. Kotliar, and P. Dai, Nat Commun **4**, 2874 (2013).

[20] V. Mishra, D.J. Scalapino, and T.A. Maier, Scientific Reports **6**, 32078 (2016).

[21] A. Linscheid, S. Maiti, Y. Wang, S. Johnston, and P.J. Hirschfeld, Phys. Rev. Lett. **117**, 077003 (2016).

[22] Z. P. Yin, K. Haule, and G. Kotliar, Nat. Mater. **10**, 932 (2011).

[23] L. de Medici, G. Giovannetti, and M. Capone, Phys. Rev. Lett. **112**, 177001 (2014).

[24] A. Kreisel, B. M. Andersen, P. O. Sprau, A. Kostin, J. C. S. Davis, and P. J. Hirschfeld, Phys. Rev. B **95**, 174504 (2017).

[25] P. O. Sprau, A. Kostin, A. Kreisel, A. E. Bhmer, V. Taufour, P. C. Canfield, S. Mukherjee, P. J. Hirschfeld, B. M. Andersen, Science **357**, 75 (2017).

[26] J. Zhao, D.-X. Yao, S. Li, T. Hong, Y. Chen, S. Chang, W. Ratliff, J. W. Lynn, H. A. Mook, G. F. Chen, J. L. Luo, N. L. Wang, E. W. Carlson, J. Hu, and P. Dai, Phys. Rev. Lett. **101**, 167203 (2008).

[27] Q. Wang, Y. Shen, B. Pan, X. Zhang, K. Ikeuchi, K. Iida, A. D. Christianson, H. C. Walker, D. T. Adroja, M. Abdel-Hafiez, X. Chen, D. A. Chareev, A. N. Vasiliev, and J. Zhao, Nat. Comm. **7**, 12182 (2016).

[28] Y. Li, Z. Yin, X. Wang, D. W. Tam, D. L. Abernathy, A. Podlesnyak, C. Zhang, M. Wang, L. Xing, C. Jin, K. Haule, G. Kotliar, T. A. Maier, and P. Dai, Phys. Rev. Lett. **116**, 247001 (2016).